PCCP

PAPER

View Article Online
View Journal | View Issue

Cite this: *Phys. Chem. Chem. Phys.*, 2019, **21**, 7924

Rethinking the $X^- + CH_3Y$ [X = OH, SH, CN, NH_2, PH_2; Y = F, Cl, Br, I] S_N2 reactions†

Domonkos A. Tasi, Zita Fábián and Gábor Czakó *

Received 27th December 2018,
Accepted 15th March 2019

DOI: 10.1039/c8cp07850e

rsc.li/pccp

Moving beyond the textbook mechanisms of bimolecular nucleophilic substitution (S_N2) reactions, we characterize several novel stationary points and pathways for the reactions of X^- [X = OH, SH, CN, NH_2, PH_2] nucleophiles with CH_3Y [Y = F, Cl, Br, I] molecules using the high-level explicitly-correlated CCSD(T)-F12b method with the aug-cc-pV*n*Z(-PP) [*n* = D, T, Q] basis sets. Besides the not-always-existing traditional pre- and post-reaction ion-dipole complexes, $X^-\cdots H_3CY$ and $XCH_3\cdots Y^-$, and the Walden-inversion transition state, $[X–CH_3–Y]^-$, we find hydrogen-bonded $X^-\cdots HCH_2Y$ (X = OH, CN, NH_2; Y ≠ F) and front-side $H_3CY\cdots X^-$ (Y ≠ F) complexes in the entrance and hydrogen-bonded $XH_2CH\cdots Y^-$ (X = SH, CN, PH_2) and $H_3CX\cdots Y^-$ (X = OH, SH, NH_2) complexes in the exit channels depending on the nucleophile and leaving group as indicated in parentheses. Retention pathways *via* either a high-energy front-side attack barrier, $XYCH_3^-$, or a novel double-inversion transition state, $XH\cdots CH_2Y^-$, having lower energy for X = OH, CN, and NH_2 and becoming submerged (barrier-less) for X = OH and Y = I as well as X = NH_2 and Y = Cl, Br, and I, are also investigated.

I. Introduction

Since the discovery of an optical inversion in a chemical reaction by Paul Walden in 1896,[1] bimolecular nucleophilic substitution (S_N2) has become a widely known reaction class in organic chemistry. The atomic-level mechanisms of S_N2 reactions were already described in the 1930s by Ingold and co-workers.[2] The traditional S_N2 Walden-inversion pathway goes through a double-well potential featuring ion-dipole complexes in the entrance- and exit-channel wells separated by a central transition state (first-order saddle point). In a typical S_N2 reaction $X^- + CH_3Y$, the nucleophile (X^-) attacks the back side (methyl side) of the CH_3Y molecule and while a new X–C bond forms and the C–Y bond breaks an umbrella motion of the H atoms inverts the configuration around the carbon center. The above-described Walden-inversion mechanism of S_N2 reactions has become textbook material and is probably the best-known stereo-specific reaction pathway in chemistry. However, in 2016 Xie and Hase[3] published a perspective article "rethinking the S_N2 reaction", because "the gas-phase dynamics of a paradigm organic reaction are more complex than expected". This statement on the complexity of S_N2 reactions was based on recent experimental and theoretical findings revealing several novel and unexpected reaction mechanisms for these paradigm systems.[4–9] For example, S_N2 reactions can proceed with direct rebound, stripping, and front-side attack mechanisms as well as *via* indirect ion-dipole, hydrogen-bond, and front-side complex forming, roundabout,[4] and double-inversion[7] pathways.[3] Among the above mechanisms front-side attack is a retention pathway, which proceeds *via* a high-energy $XYCH_3^-$-like transition state with X–C–Y angle of around 80°.[10] This front-side attack retention pathway has been known from the early 1930s;[2] however, a quantitative description of the front-side attack dynamics was just recently achieved in our group utilizing newly developed analytical *ab initio* potential energy surfaces.[7,11,12] Furthermore, our reaction dynamics simulations on these analytical potentials revealed a new retention mechanism called double inversion,[7] where a proton-abstraction induced inversion (first inversion) is followed by a Walden inversion (second inversion) resulting in retention of the initial configuration. The non-traditional front-side complex ($H_3CY\cdots X^-$) formation was also quantitatively characterized by our trajectory simulations[13] motivated by the joint work with the experimental group of Wester and co-workers.[8] Another non-traditional pre-reaction complex stabilized by a hydrogen-bond between X^- and the methyl group of CH_3Y was also found first by Hase and co-workers[14] and later in our theoretical studies.[7,11,12,15]

In the present work we focus on "rethinking" the gas-phase $X^- + CH_3Y$ [X = OH, SH, CN, NH_2, PH_2; Y = F, Cl, Br, I] S_N2 reactions using high-level *ab initio* methods. Among the 20 possible fundamental S_N2 reactions with the above-defined 5 different nucleophiles (X^-) and 4 leaving groups (Y), there are

Interdisciplinary Excellence Centre and Department of Physical Chemistry and Materials Science, Institute of Chemistry, University of Szeged, Rerrich Béla tér 1, Szeged H-6720, Hungary. E-mail: gczako@chem.u-szeged.hu

† Electronic supplementary information (ESI) available: All the structural parameters, harmonic frequencies, absolute energies, and relative energies of the stationary points as well as Cartesian coordinates of the best geometries. See DOI: 10.1039/c8cp07850e

only a few which were studied previously in the gas[16–24] and/or condensed[25–29] phases, and almost none of them in view of the recent non-traditional mechanisms. Focusing on the gas-phase studies, in the case of Y = F Gonzales *et al.*[16,17] characterized 3 stationary points, *i.e.*, pre- and post-reaction complexes and a Walden-inversion transition state, for each reaction; however, front-side complex formation, a front-side attack transition state, and double inversion were not investigated, partially due to the fact that some of these were not known at that time. For OH^- + CH_3F Hase and co-workers[18,19] described the same 3 stationary points as Gonzales *et al.*[16,17] and reported interesting direct dynamics results showing that trajectories usually avoid the deep post-reaction minimum.[18] Considering ligands other than Y = F, Tachikawa and co-workers[20] investigated again 3 stationary points for the OH^- + CH_3Cl reaction and recently Wester and co-workers[21] reported crossed-beam experiments for the CN^- + CH_3I system and characterized 3 stationary points for each of the C–C and C–N bond forming S_N2 reactions. In the case of X = OH and SH, the X^- + CH_3Y [Y = F, Cl, Br] reactions were investigated by Longo and co-workers[22] reporting again 3 stationary points for each system. Perhaps the most thoroughly studied reaction is OH^- + CH_3I, for which H-bonded and front-side complex formation were studied in the Hase group[24] and experiments were performed in the groups of Viggiano[23] and Wester.[24] In 2018 we reported a high-level *ab initio* study on the OH^- + CH_3Y [Y = F, Cl, Br, I] S_N2 reactions applying core- and post-CCSD(T) correlation corrections, which are usually neglected in the literature, and revealing many stationary points involving H-bonded and front-side complexes as well as front-side attack and double-inversion transition states.[30] In the present work we extend our previous studies[9,30] considering SH^-, CN^-, NH_2^-, and PH_2^- nucleophiles besides OH^-, which is described again for completeness and comparison. For the first time for X = SH, CN, NH_2, and PH_2 we use the high-level modern explicitly-correlated CCSD(T)-F12b method[31] to obtain benchmark structures and relative energies for the stationary points. However, instead of presenting technical details of a high-level electronic structure study, the present work aims to provide new qualitative insights into the reaction pathways of 20 different S_N2 reactions, showing that these systems "are more complex than expected",[3] supporting the views of the above-mentioned "rethinking" perspective article.[3]

II. Computational details

The energies, geometries, and harmonic vibrational frequencies of the stationary points are computed using second-order Møller–Plesset perturbation theory[32] (MP2) with the correlation-consistent aug-cc-pVDZ basis set[33] and the explicitly correlated coupled cluster singles, doubles, and perturbative triples CCSD(T)-F12b method[31] with the aug-cc-pVDZ and the aug-cc-pVTZ basis sets.[33] To obtain the benchmark classical relative energies at the CCSD(T)-F12b/aug-cc-pVTZ geometries single-point computations are performed using the CCSD(T)-F12b method with the quadruple-ζ aug-cc-pVQZ basis set.[33] For bromine and iodine relativistic small-core effective core potentials[34] and the corresponding pseudo-potential basis sets[34] are employed.

The benchmark adiabatic relative energies are determined as:

$$\Delta E[\text{CCSD(T)-F12b/aug-cc-pVQZ}] + \Delta\text{ZPE}[\text{CCSD(T)-F12b/aug-cc-pVTZ}] \quad (1)$$

where ΔE is the benchmark classical relative energy and ΔZPE is the harmonic zero-point energy correction. Note that if the CCSD(T)-F12b/aug-cc-pVTZ or the CCSD(T)-F12b/aug-cc-pVDZ geometry optimizations do not converge the CCSD(T)-F12b/aug-cc-pVDZ or the MP2/aug-cc-pVDZ structures are utilized, respectively.

All the structural parameters, harmonic frequencies, absolute energies, and relative energies can be found in the ESI.† For the best stationary-point geometries Cartesian coordinates are also given in the ESI† in a software-friendly format. We note that in the case of some minima small artificial imaginary frequencies ($<100i$ cm^{-1}) are found most likely due to the uncertainty of the numerical gradient and/or Hessian computations. For the present *ab initio* study the Molpro program package[35] is used.

III. Results and discussion

OH^- + CH_3Y [Y = F, Cl, Br, I]

The OH^- + CH_3Y [Y = F, Cl, Br, I] S_N2 reactions are exothermic and may proceed *via* back-side attack inversion, front-side attack retention, or double-inversion retention pathways as shown in Fig. 1. Back-side attack is a collective name for several direct and indirect inversion mechanisms such as rebound, stripping, ion-dipole complex formation, hydrogen-bond complex formation, front-side complex formation, and roundabout. The traditional picture says that back-side attack Walden inversion proceeds *via* a pre-reaction ion-dipole complex (PreMIN), a Walden-inversion transition state (WaldenTS), and a post-reaction ion-dipole complex $HOCH_3\cdots Y^-$. However, instead of the traditional $HOCH_3\cdots Y^-$ complex, Y^- connects to the OH group with a single hydrogen bond forming a PostHMIN complex for all the four leaving groups, as shown in Fig. 1. Thus, Walden inversion of OH^- + CH_3F proceeds as PreMIN → WaldenTS → PostHMIN. (Note that besides PostHMIN a hydrogen-bonded $F^-\cdots HCH_2OH$ complex also exists, which is not shown in Fig. 1, but presented in the ESI.†) This is not the end of the nontraditional mechanisms, because for Y = Cl, Br, and I a hydrogen-bonded pre-reaction complex (HMIN), where OH^- connects to one of the H atoms of the methyl group, and a transition state (HTS) connecting HMIN and PREMIN come into play, where HMIN is below PREMIN by about 2 kcal mol^{-1}. In the case of Y = Cl and Br, OH^- + CH_3Y Walden inversion occurs *via* HMIN → HTS → PreMIN → WaldenTS → PostHMIN. However, for Y = I the traditional PreMIN and WaldenTS do not exist and the OH^- + CH_3I inversion proceeds as HMIN → HTS → PostHMIN. Furthermore, for Y = Cl, Br, and I a front-side complex (FSMIN), where OH^- connects to Y, can also be found, which in the case of Y = I is actually a significantly deeper minimum than HMIN, suggesting a steering effect into a nonreactive orientation,

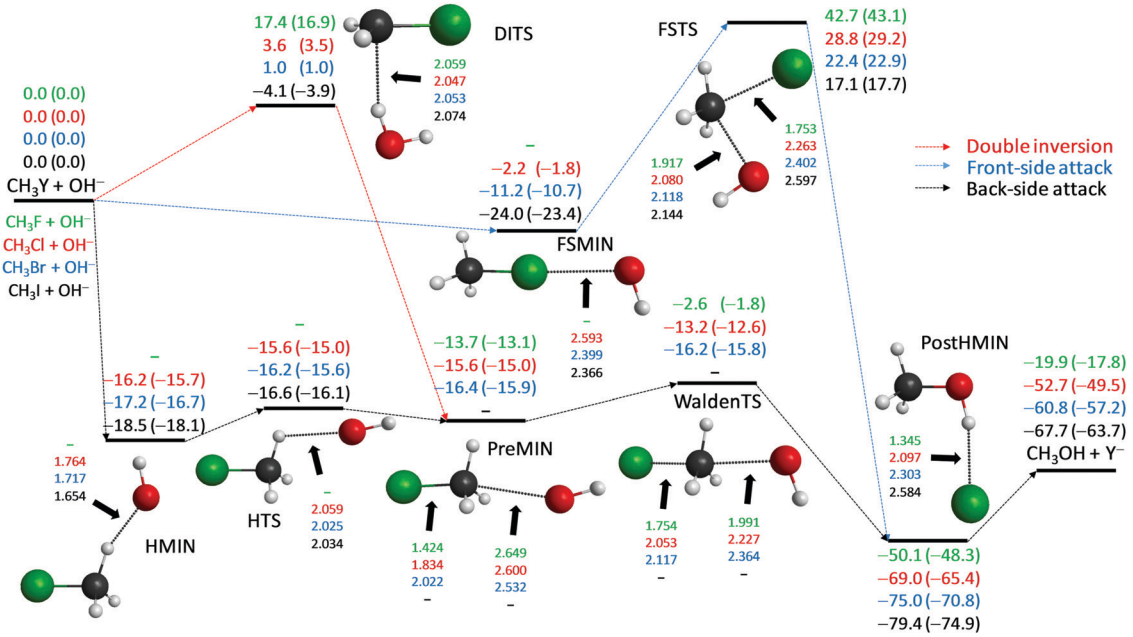

Fig. 1 Schematic potential energy surfaces of the OH^- + CH_3Y [Y = F, Cl, Br, I] S_N2 reactions showing the classical (adiabatic) CCSD(T)-F12b/aug-cc-pVQZ (+ΔZPE[CCSD(T)-F12b/aug-cc-pVTZ]) relative energies, in kcal mol^{-1}, and the most important CCSD(T)-F12b/aug-cc-pVTZ structural parameters, in Å, of the stationary points along the different reaction pathways. For core and post-CCSD(T) correlation corrected energies and their comparison with experimental reaction enthalpies see ref. 30.

thereby making the OH^- + CH_3I reaction indirect as previous experiments[5,8] and our dynamics simulations[13] suggested for F^- + CH_3I. Unlike back-side attack inversion which has submerged stationary points, front-side attack retention proceeds *via* a high-energy transition state (FSTS) with adiabatic barrier heights of 43.1 (F), 29.2 (Cl), 22.9 (Br), and 17.7 (I) kcal mol^{-1}, whereas the corresponding double-inversion transition state (DITS) barrier heights are only 16.9 (F), 3.5 (Cl), 1.0 (Br), and −3.9 (I) kcal mol^{-1}. Thus, double inversion opens a barrier-less retention pathway for the OH^- + CH_3I S_N2 reaction.

SH^- + CH_3Y [Y = F, Cl, Br, I]

If we replace the OH^- nucleophile with SH^-, the S_N2 reactions become less exothermic and, moreover, endothermic for Y = F, as shown in Fig. 2. Unlike OH^-, SH^- does not form a hydrogen-bonded pre-reaction complex, except for Y = I as shown in the ESI,† and the back-side attack inversion pathway proceeds as PreMIN → WaldenTS → PostHMIN. The WaldenTSs are below the reactants by 1.4, 6.0, and 8.5 kcal mol^{-1}, for Y = Cl, Br, and I, respectively, whereas the SH^- + CH_3F S_N2 reaction has a positive adiabatic barrier height of 13.7 kcal mol^{-1}. Similar to the reactions of OH^-, the global minimum of the potential energy surfaces of the SH^- + CH_3Y systems is PostHMIN, but in the present case $Y^-\cdots$HC bonded (PostHMIN2) and traditional ion-dipole post-reaction (WaldenPostMIN) complexes are also found with similar energies within 1 kcal mol^{-1} and above POSTHMIN by a few kcal mol^{-1}, except for Y = F, where PostHMIN2 is just slightly bonded and WaldenPostMIN does not exist, as shown in Fig. 2. The dissociation energies of the PostHMIN complexes are around 10 kcal mol^{-1} for Y = Cl, Br, and I, whereas much larger, about 38 kcal mol^{-1}, for Y = F. In the case of X = OH, the Y = Cl, Br, and I PostHMIN complexes are more stable by a few kcal mol^{-1}, however, the Y = F complex has a dissociation energy of only about 30 kcal mol^{-1}. These energy trends are in accord with the $Y^-\cdots$HX distances, as these are slightly longer for X = SH than OH if Y = Cl, Br, and I, whereas the $F^-\cdots$HS distance (0.985 Å) is significantly shorter than the $F^-\cdots$HO distance (1.345 Å) as shown in Fig. 1 and 2. Similar to the OH^- + CH_3Y [Y = Cl, Br, I] reactions, FSMIN complexes are also found for X = SH systems, but with longer $Y\cdots X^-$ distances and consequently with less stability. Here the $H_3CI\cdots SH^-$ complex is just similarly stable to PreMIN, whereas FSMIN is a significantly deeper minimum than PREMIN in the case of the OH^- complex. We find qualitatively similar DITS and FSTS structures for the reactions of OH^- and SH^-, with significantly higher barrier heights for SH^-. Furthermore, unlike in the case of the OH^- systems, the DITSs of the SH^- nucleophile are always above the corresponding FSTSs.

CN^- + CH_3Y [Y = F, Cl, Br, I]

The CN^- nucleophile can form either a C–C or a C–N bond in the S_N2 reactions with the CH_3Y molecules. In the present work we study the energetically favored, more exothermic C–C bond formation channel leading to Y^- + CH_3CN products. The CN^- + CH_3Y reactions are more and less exothermic than the corresponding SH^- and OH^- reactions, respectively. Since the CN ligand does not have a hydrogen atom, PostHMIN-type post-reaction complexes do not exist. Here the global minimum is either a traditional ion-dipole WaldenPostMIN (C_{3v} symmetry) or a hydrogen-bonded PostHMIN2 (C_s symmetry) complex,

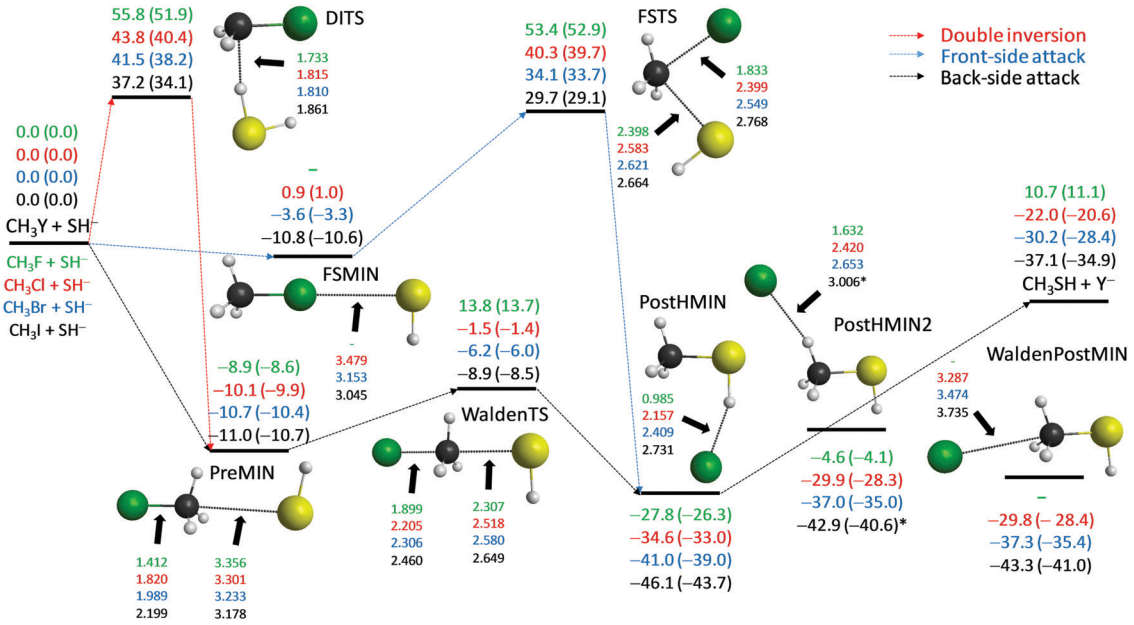

Fig. 2 Schematic potential energy surfaces of the SH^- + CH_3Y [Y = F, Cl, Br, I] S_N2 reactions showing the classical (adiabatic) CCSD(T)-F12b/aug-cc-pVQZ (+ΔZPE[CCSD(T)-F12b/aug-cc-pVTZ]) relative energies, in kcal mol^{-1}, and the most important CCSD(T)-F12b/aug-cc-pVTZ structural parameters, in Å, of the stationary points along the different reaction pathways. Results indexed by * correspond to CCSD(T)-F12b/aug-cc-pVDZ structures.

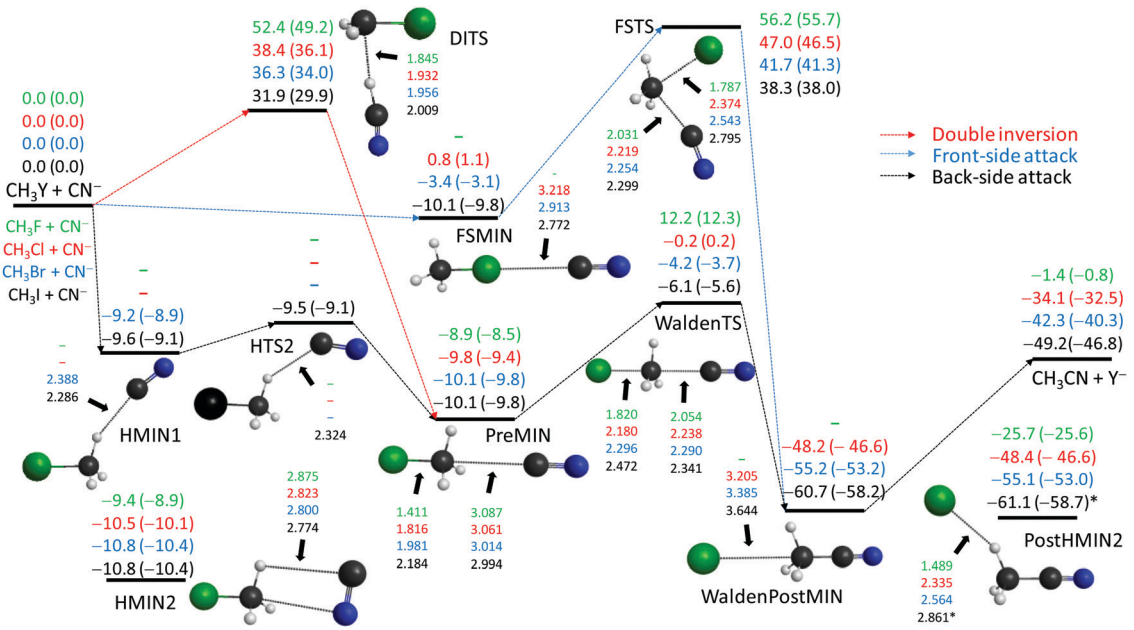

Fig. 3 Schematic potential energy surfaces of the CN^- + CH_3Y [Y = F, Cl, Br, I] S_N2 reactions showing the classical (adiabatic) CCSD(T)-F12b/aug-cc-pVQZ (+ΔZPE[CCSD(T)-F12b/aug-cc-pVTZ]) relative energies, in kcal mol^{-1}, and the most important CCSD(T)-F12b/aug-cc-pVTZ structural parameters, in Å, of the stationary points along the different reaction pathways. Results indexed by * correspond to MP2/aug-cc-pVDZ structures.

whose energies agree within 1 kcal mol^{-1} as shown in Fig. 3. Note that for Y = F, only PostHMIN2 is found. Traditional PreMINs and WaldenTSs are found for all the four leaving groups and unlike in the case of OH^- and SH^-, these stationary points have C_{3v} symmetry with collinear Y–C–C–N arrangements. WaldenTSs are clearly submerged for Y = Br and I with classical (adiabatic) energies of −4.2 (−3.7) and −6.1 (−5.6) kcal mol^{-1}, respectively, relative to the reactants. For Y = Cl the barrier height is close to zero, *i.e.* −0.2 (0.2) kcal mol^{-1}, whereas for Y = F Walden inversion has a positive barrier of 12.2 (12.3) kcal mol^{-1}, similar to the SH^- + CH_3F reaction. Besides the ion-dipole PreMIN complexes, we find hydrogen-bonded complexes (HMIN1) for Y = Br and I and a transition state connecting HMIN1 and PreMIN for Y = I as seen in Fig. 3. Unlike in the OH^- case, here HMIN1 is

slightly above PreMIN. Furthermore, for all the four CN^- + CH_3Y systems we find pre-reaction complexes (HMIN2), where the C and N atoms of CN^- are connected to the H and C atoms of CH_3Y, respectively, as seen in Fig. 3. These HMIN2 complexes are slightly more stable than the PREMINs; thus, HMIN2 configurations are the deepest regions of the entrance channels. Similar to the OH^- and SH^- reactions, front-side FSMIN complexes are found for Y = Cl, Br, and I, but unlike in the former cases, the $H_3CY\cdots CN^-$ complexes have C_{3v} symmetry. In the Y = I case the depth of FSMIN is similar, 10 ± 1 kcal mol^{-1}, to the other minima in the entrance channel, whereas for Y = Br the classical (adiabatic) FSMIN depth is only 3.4 (3.1) kcal mol^{-1}. For Y = Cl FSMIN is unbonded, with an energy slightly above the reactant asymptote. The retention pathways have large barriers between 30 and 60 kcal mol^{-1} depending on the leaving group. Similar to the OH^- + CH_3Y systems, DITSs are always below the corresponding FSTSs, but whereas the OH^- + CH_3I reaction has a negative double-inversion barrier, the classical (adiabatic) barrier height of the CN^- + CH_3I reaction is 31.9 (29.9) kcal mol^{-1}.

NH_2^- + CH_3Y [Y = F, Cl, Br, I]

The S_N2 reactions of NH_2^- with CH_3Y are the most exothermic among the systems studied in this work; the enthalpies of the NH_2^- + CH_3Y reactions are more negative by 15–20 kcal mol^{-1} than those of the corresponding, also highly exothermic OH^- + CH_3Y processes. Similar to the reactions of OH^-, the global minima of the NH_2^- + CH_3Y potential energy surfaces correspond to PostHMIN complexes, where Y^- is connected to the NH_2 group of CH_3NH_2 with a single hydrogen bond as seen in Fig. 4. The D_e (D_0) dissociation energies of the $CH_3NH_2\cdots Y^-$ complexes are 18.2 (17.9), 10.0 (9.5), 8.7 (8.3), and 7.3 (7.0) kcal mol^{-1} for Y = F, Cl, Br, and I, respectively, whereas the corresponding D_e (D_0) values of $CH_3OH\cdots Y^-$ are 30.2 (30.5), 16.3 (15.9), 14.2 (13.6), and 11.7 (11.2) kcal mol^{-1}, in order. The lower stability of the $CH_3NH_2\cdots Y^-$ complexes is in accord with the longer $NH\cdots Y^-$ bond lengths of 1.579 (F), 2.330 (Cl), 2.539 (Br), and 2.826 (I) Å with respect to the corresponding 1.345 (F), 2.097 (Cl), 2.303 (Br), and 2.584 (I) Å values of the OH systems. The back-side attack NH_2^- + CH_3F S_N2 reaction proceeds *via* the PreMIN → WaldenTS → PostHMIN inversion pathway featuring a slightly submerged transition state with a classical (adiabatic) energy of −3.0 (−1.9) kcal mol^{-1} relative to the reactants. For Y = Cl a hydrogen-bonded pre-reaction complex (HMIN) is also found with similar energy, around −14 kcal mol^{-1}, to that of PreMIN and WaldenTS is at −12.8 (−12.1) kcal mol^{-1}. In the case of Y = Br we could not find a WaldenTS, and HMIN is deeper than PreMIN by about 1 kcal mol^{-1}. For Y = I neither a traditional PreMIN nor WaldenTS is found, but HMIN and a pre-reaction transition state (PreTS) exist as seen in Fig. 4. The submerged PreTS with a classical (adiabatic) energy of −15.6 (−15.2) kcal mol^{-1} relative to the reactants differs from WaldenTS in the orientation of the NH_2 unit and the relative stretching of the C–Y distance, because C–F and C–Cl WaldenTS distances are stretched by 0.324 and 0.220 Å relative to the corresponding bond lengths of the CH_3Y molecule, whereas the C–I PreTS distance is just longer by 0.107 Å than the same bond in CH_3I. Therefore, PreTS may be viewed as an early WaldenTS. As always front-side complexes are found for Y = Cl, Br, and I with D_e (D_0) dissociation energies of 1.7 (1.1), 12.5 (11.5), and 25.8 (24.4) kcal mol^{-1}, respectively. Thus, the stability of the front-side complex is negligible for Y = F, comparable to that of HMIN in the case of Y = Br, and

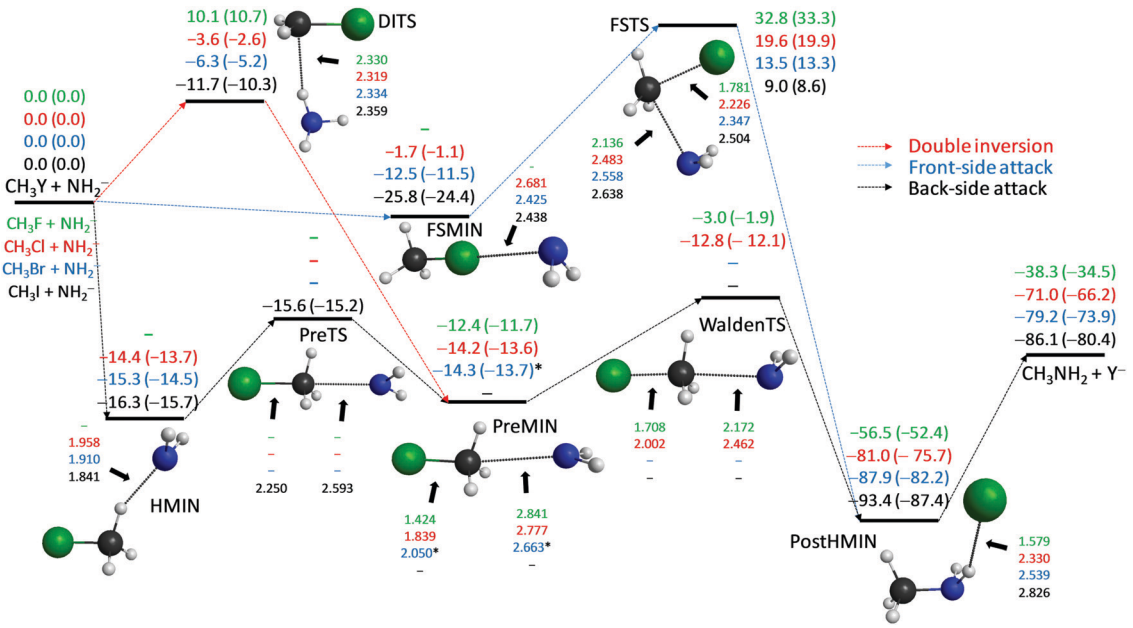

Fig. 4 Schematic potential energy surfaces of the NH_2^- + CH_3Y [Y = F, Cl, Br, I] S_N2 reactions showing the classical (adiabatic) CCSD(T)-F12b/aug-cc-pVQZ (+ΔZPE[CCSD(T)-F12b/aug-cc-pVTZ]) relative energies, in kcal mol^{-1}, and the most important CCSD(T)-F12b/aug-cc-pVTZ structural parameters, in Å, of the stationary points along the different reaction pathways. Results indexed by * correspond to MP2/aug-cc-pVDZ structures. "Experimental" 0 K reaction enthalpies, with ±0.1 kcal mol^{-1} uncertainties, are −34.7, −66.1, −73.7, and −79.9 kcal mol^{-1} for Y = F, Cl, Br, and I, respectively.[36]

significantly stronger than that of HMIN for Y = I. Note that $H_3CI\cdots NH_2^-$ is the most strongly bonded front-side complex investigated in the present study. The retention pathways of the title reactions are the most favored in the case of the NH_2^- nucleophile. All the DITS and FSTS barrier heights are below the corresponding, also favorable, OH^- barriers by about 10 kcal mol^{-1}. Furthermore, all the DITS barriers are below the corresponding FSTS ones by about 20 kcal mol^{-1}; thus, double inversion opens a significantly lower energy retention pathway compared to the more traditional front-side attack. Moreover, for Y = Cl, Br, and I double inversion has negative classical (adiabatic) barrier heights of −3.6 (−2.6), −6.3 (−5.2), and −11.7 (−10.3) kcal mol^{-1}, respectively, opening retention pathways which may become competitive with inversion especially for the iodine leaving group.

PH_2^- + CH_3Y [Y = F, Cl, Br, I]

The PH_2^- + CH_3Y reactions are less exothermic than the analogous NH_2^- + CH_3Y systems due to the weaker C–P bonds compared to the binding energy of a C–N bond. For the reactions of PH_2^- we find a PostHMIN complex only for Y = F; however, its structure differs from the geometry of the PostHMIN complexes of the other nucleophiles. Here, the P···H distance is significantly stretched, whereas the F–H distance is close to the bond length in the HF molecule; thus, this PostHMIN is better viewed as a post-reaction proton-abstraction (proton transfer from the PH_2 group to F^-) complex. For all the four leaving groups we find hydrogen-bonded complexes in the exit channel (PostHMIN2), where Y^- connects to one of the H atoms of the methyl group as seen in Fig. 5. Note that the proton-abstraction-like PostHMIN, found for Y = F, is a deeper minimum than PostHMIN2, but the enthalpy of the HF + CH_3PH^- channel (−8.4 kcal mol^{-1}) is less exothermic than that corresponding to the F^- + CH_3PH_2 S_N2 products (−10.3 kcal mol^{-1}). A traditional ion-dipole complex (WaldenPostMIN) is only found for Y = Br, but with slightly less stability than the corresponding PostHMIN2. In the entrance channel hydrogen-bonded complexes are not found unlike for the analogous NH_2^- reactions. For Y = F, Cl, and Br traditional ion-dipole complexes (PreMIN) and WaldenTSs are found as shown in Fig. 5. Note that in the Y = F case the Walden-inversion pathway has a positive classical (adiabatic) barrier of 9.7 (9.8) kcal mol^{-1}, whereas WaldenTSs are submerged for Y = Cl and Br. For Y = Cl, Br, and I we find PreTSs similar to the Y = I case of the NH_2^- reactions. For Y = I PreTS is the only entrance-channel stationary point with a reactive orientation. Front-side complexes (FSMIN) are found for Y = Cl, Br, and I, but in the case of Y = Cl the stationary point has a slightly positive energy relative to the reactants. The $H_3CI\cdots PH_2^-$ complex has D_e (D_0) values of 13.8 (13.5) kcal mol^{-1}; thus, this configuration is the global minimum of the entrance channel similarly to the OH^- and NH_2^- + CH_3I reactions. The retention pathways of the PH_2^- + CH_3Y reactions proceed *via* high barriers and, unlike in the OH^- and NH_2^- reactions, DITSs are slightly above the FSTSs similarly to the SH^- systems.

IV. Summary and conclusions

Motivated by a recent perspective article entitled "Rethinking the S_N2 reaction"[3] and our previous findings about a novel double-inversion[7] pathway and front-side complex formation,[13] we have investigated the stationary points and possible reaction mechanisms of 20 different gas-phase S_N2 reactions involving

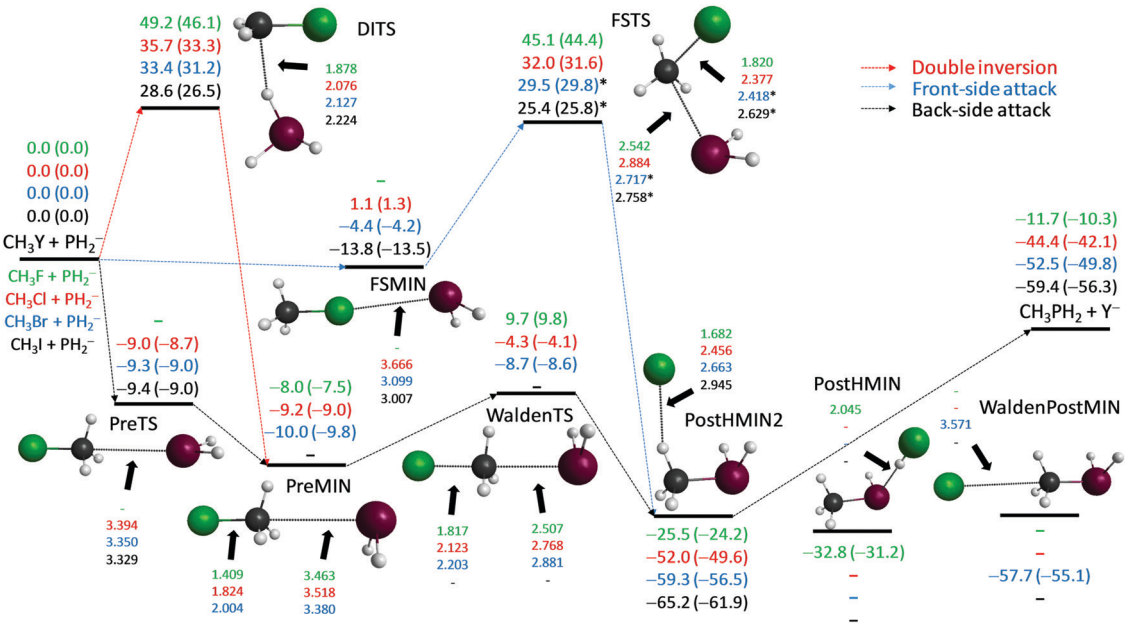

Fig. 5 Schematic potential energy surfaces of the PH_2^- + CH_3Y [Y = F, Cl, Br, I] S_N2 reactions showing the classical (adiabatic) CCSD(T)-F12b/aug-cc-pVQZ (+ΔZPE[CCSD(T)-F12b/aug-cc-pVTZ]) relative energies, in kcal mol^{-1}, and the most important CCSD(T)-F12b/aug-cc-pVTZ structural parameters, in Å, of the stationary points along the different reaction pathways. Results indexed by * correspond to MP2/aug-cc-pVDZ structures.

OH^-, SH^-, CN^-, NH_2^-, and PH_2^- nucleophiles and methyl-halide molecules (CH_3Y, Y = F, Cl, Br, I). Previous work usually reported three stationary points, *i.e.*, pre- and post-reaction complexes and a central transition state, for some of these S_N2 systems. In the present comprehensive high-level explicitly-correlated *ab initio* study we reveal that these reactions are much more complex and many stationary points play a role in the dynamics. In the entrance channel, besides the traditional ion-dipole complex and Walden-inversion transition state, hydrogen-bonded and front-side complexes are found. Pre-reaction hydrogen-bond formation usually occurs between OH^-, CN^-, and NH_2^- nucleophiles and CH_3Y, where Y = Cl, Br, and I, and the hydrogen-bonded complex is more stable than the traditional ion-dipole complex for OH^- and NH_2^-. Front-side complexes, where the nucleophile connects to the leaving group, are found in all cases except Y = F. For X = OH, NH_2, and PH_2, the $H_3CI\cdots X^-$ complex is the deepest region in the entrance channel suggesting indirect dynamics, because the deep front-side minimum may steer the reactants into a non-reactive orientation. In the exit channel a hydrogen-bonded $H_3CX\cdots Y^-$ complex may be formed for X = OH, SH, and NH_2, which is the global minimum of the potential energy surface. In the case of X = CN and PH_2, the Y^- rather forms a hydrogen bond with one of the H atoms of the methyl group or in some cases a traditional ion-dipole complex is also found. Besides the Walden-inversion mechanisms, we report, in most cases for the first time, front-side attack and double-inversion retention pathways for the title reactions. Front-side attack always has a positive, usually large, barrier, whereas the double-inversion barrier heights are below the front-side attack ones in the case of the OH^-, CN^-, and NH_2^- nucleophiles. Moreover, for the OH^- + CH_3I and the NH_2^- + CH_3Y [Y = Cl, Br, I] reactions the double-inversion transition state is submerged, thereby opening a barrier-less retention pathway for these S_N2 reactions. We hope that the present study motivates future experimental and theoretical investigations on the dynamics of the title reactions and shapes the way how we think about S_N2 reactions.

Conflicts of interest

There are no conflicts of interest to declare.

Acknowledgements

This work was supported by the National Research, Development and Innovation Office – NKFIH, K-125317 and the Ministry of Human Capacities, Hungary grant 20391-3/2018/FEKUSTRAT. D. A. T. is thankful for support from the National Young Talent Scholarship (NTP-NFTÖ-18-B-0399).

References

1 P. Walden, *Ber. Dtsch. Chem. Ges.*, 1896, **29**, 133.
2 W. A. Cowdrey, E. D. Hughes, C. K. Ingold, S. Masterman and A. D. Scott, *J. Chem. Soc.*, 1937, 1252.
3 J. Xie and W. L. Hase, *Science*, 2016, **352**, 32.
4 J. Mikosch, S. Trippel, C. Eichhorn, R. Otto, U. Louderaj, J.-X. Zhang, W. L. Hase, M. Weidemüller and R. Wester, *Science*, 2008, **319**, 183.
5 J. Mikosch, J. Zhang, S. Trippel, C. Eichhorn, R. Otto, R. Sun, W. A. de Jong, M. Weidemüller, W. L. Hase and R. Wester, *J. Am. Chem. Soc.*, 2013, **135**, 4250.
6 J. Xie, R. Otto, J. Mikosch, J. Zhang, R. Wester and W. L. Hase, *Acc. Chem. Res.*, 2014, **47**, 2960.
7 I. Szabó and G. Czakó, *Nat. Commun.*, 2015, **6**, 5972.
8 M. Stei, E. Carrascosa, M. A. Kainz, A. H. Kelkar, J. Meyer, I. Szabó, G. Czakó and R. Wester, *Nat. Chem.*, 2016, **8**, 151.
9 I. Szabó and G. Czakó, *J. Phys. Chem. A*, 2017, **121**, 9005.
10 I. Szabó and G. Czakó, *J. Phys. Chem. A*, 2015, **119**, 3134.
11 I. Szabó, H. Telekes and G. Czakó, *J. Chem. Phys.*, 2015, **142**, 244301.
12 B. Olasz, I. Szabó and G. Czakó, *Chem. Sci.*, 2017, **8**, 3164.
13 I. Szabó, B. Olasz and G. Czakó, *J. Phys. Chem. Lett.*, 2017, **8**, 2917.
14 J. Zhang, J. Mikosch, S. Trippel, R. Otto, M. Weidemüller, R. Wester and W. L. Hase, *J. Phys. Chem. Lett.*, 2010, **1**, 2747.
15 I. Szabó, A. G. Császár and G. Czakó, *Chem. Sci.*, 2013, **4**, 4362.
16 J. M. Gonzales, R. S. Cox, S. T. Brown, W. D. Allen and H. F. Schaefer, *J. Phys. Chem. A*, 2001, **105**, 11327.
17 J. M. Gonzales, C. Pak, R. S. Cox, W. D. Allen, H. F. Schaefer III, A. G. Császár and G. Tarczay, *Chem. – Eur. J.*, 2003, **9**, 2173.
18 L. Sun, K. Song and W. L. Hase, *Science*, 2002, **296**, 875.
19 L. Sun, K. Song, W. L. Hase, M. Sena and J. M. Riveros, *Int. J. Mass Spectrom.*, 2003, **227**, 315.
20 H. Tachikawa, M. Igarashi and T. Ishibashi, *J. Phys. Chem. A*, 2002, **106**, 10977.
21 E. Carrascosa, M. Bawart, M. Stei, F. Linden, F. Carelli, J. Meyer, W. D. Geppert, F. A. Gianturco and R. Wester, *J. Chem. Phys.*, 2015, **143**, 184309.
22 Y. G. Proenza, M. A. F. de Souza and R. L. Longo, *Chem. – Eur. J.*, 2016, **22**, 16220.
23 J. Xie, S. C. Kohale, W. L. Hase, S. G. Ard, J. J. Melko, N. S. Shuman and A. A. Viggiano, *J. Phys. Chem. A*, 2013, **117**, 14019.
24 J. Xie, R. Sun, M. R. Siebert, R. Otto, R. Wester and W. L. Hase, *J. Phys. Chem. A*, 2013, **117**, 7162.
25 J. Chen, Y. Xu and D. Wang, *J. Comput. Chem.*, 2014, **35**, 445.
26 H. Yin, D. Wang and M. Valiev, *J. Phys. Chem. A*, 2011, **115**, 12047.
27 Y. Xu, T. Wang and D. Wang, *J. Chem. Phys.*, 2012, **137**, 184501.
28 Y. Xu., J. Zhang and D. Wang, *Phys. Chem. Chem. Phys.*, 2014, **16**, 19993.
29 Y. Xu., J. Zhang and D. Wang, *J. Chem. Phys.*, 2015, **142**, 244505.
30 D. A. Tasi, Z. Fábián and G. Czakó, *J. Phys. Chem. A*, 2018, **122**, 5773.

31 T. B. Adler, G. Knizia and H.-J. Werner, *J. Chem. Phys.*, 2007, **127**, 221106.
32 C. Møller and M. S. Plesset, *Phys. Rev.*, 1934, **46**, 618.
33 T. H. Dunning Jr., *J. Chem. Phys.*, 1989, **90**, 1007.
34 K. A. Peterson, D. Figgen, E. Goll, H. Stoll and M. Dolg, *J. Chem. Phys.*, 2003, **119**, 11113.
35 H.-J. Werner, P. J. Knowles, G. Knizia, F. R. Manby, M. Schütz *et al.*, *Molpro, version 2015.1, a package of ab initio programs*, see http://www.molpro.net.
36 B. Ruscic and D. H. Bross, Active Thermochemical Tables (ATcT) values based on ver. 1.122d of the Thermochemical-Network (2018); available at ATcT.anl.gov.